Available online at www.sciencedirect.com
SCIENCE DIRECT®
Journal of Nuclear Materials 323 (2003) 281–289
journal of nuclear materials
www.elsevier.com/locate/jnucmat

Modeling of dislocation–grain boundary interactions in FCC metals

M. de Koning [a], R.J. Kurtz [b,*], V.V. Bulatov [a], C.H. Henager [b], R.G. Hoagland [b], W. Cai [a], M. Nomura [b]

[a] *Lawrence Livermore National Laboratory, Livermore, CA 94550, USA*
[b] *Pacific Northwest National Laboratory, P.O. Box 999, Richland, WA 99352, USA*

Abstract

In this paper recent 2D and 3D computational modeling studies of the interaction between dislocations and grain boundaries (GB) in FCC metals will be presented. 2D simulations of lattice dislocation interaction with Σ11 tilt GBs in Al are presented and discussed. Studies of a Σ11 symmetric tilt GB reveal that transmitted dislocations result in local GB migration and disconnection formation. A classical elastic analysis makes correct predictions in one case but not another. Glissile GB dislocations are created in this process, which means that part of the transmitted dislocation is absorbed. Calculations of lattice dislocations interacting with a Σ11 asymmetric tilt GB show that the nature of the interaction depends on local GB structure and transmission is observed in some cases to occur on planes that do not have the highest resolved glide stress. Results of large-scale 3D molecular dynamic simulations are also described, investigating the interaction between dislocations nucleating from a crack tip and a number of symmetric tilt GBs in Ni. Using a line-tension model to analyze the data, it is found that the outcomes of dislocation–GB collisions can be rationalized in terms of only three geometrical parameters, in accordance with in situ TEM observations.

PACS: 61.72.Bb; 61.72.Mm; 62.20.Fe; 71.15.Pd

1. Introduction

Arguably the most complicated aspect of modeling the mechanical properties of crystalline solids is the fact that the deformation behavior is controlled by processes that act simultaneously on different length and time scales. Attempts to predict the mechanical behavior of a macroscopic solid based solely on an atomistic description are overwhelmingly hopeless. Rather, a multiscale modeling strategy is adopted consisting of a hierarchy of modeling techniques, each of which focuses on a particular scale. The coupling between the scales is accomplished using a set of phenomenological parameters, which must be determined through a coarse-graining or information passing procedure, in which a reduced set of variables is passed from one scale to the next.

For modeling mechanical behavior, a particularly important problem concerns the information passing involved in coupling the behavior of single-dislocations on the atomistic scale to that of modeling the evolution of large groups of dislocations by means of dislocation-dynamics simulations (DD). The conceptual approach to be followed for single-crystal plasticity is straightforward since the relevant unit processes, such as single-dislocation mobility and dislocation-junction formation/destruction, and the parameters required to characterize them are known and can be quantified using atomistic methods. For polycrystal plasticity, however, the problem is significantly more complex due to the role of grain boundaries (GB) in plastic deformation. While the interactions between lattice dislocations and GBs are

* Corresponding author. Tel.: +1-509 373 7515; fax: +1-509 376 0418.
E-mail address: rj.kurtz@pnl.gov (R.J. Kurtz).

0022-3115/$ - see front matter © 2003 Elsevier B.V. All rights reserved.
doi:10.1016/j.jnucmat.2003.08.008

considered of fundamental importance in this case, only little is known about their unit mechanisms, and even less about which of these are most relevant in the overall evolution of a given grain microstructure under an external stress. This is because of the enormous richness of possible combinations of GB geometry and dislocation character, and the wide variety of distinct outcomes of dislocation–GB collisions, including, for instance, dislocation absorption, reflection, and transmission. The number of parameters required to describe these processes is large, potentially including 5 degrees of freedom associated with the GB geometry, the Burgers vector and glide plane of the involved dislocations, the stress state on both sides of the GB plane, temperature, and possibly others.

In this context, the role of atomistic simulations may be twofold. On the one hand they serve as a tool for the comprehensive analysis of individual dislocation–GB collisions, providing detailed structural understanding of the involved atomic rearrangements, including, for instance, complete Burgers vector information of the involved dislocation reactions. On the other hand, a series of atomistic simulations can be used to explore trends in the dislocation–GB interactions for different geometries, stress conditions, and temperature, to discern which of these parameters are most relevant in determining the outcome of dislocation–GB collisions and should form the basis for the information-passing scheme linking the atomistic to higher modeling scales. In this paper we present examples of both applications. First, we describe results of a series of 2-dimensional (2D) atomistic simulations of the transmission of lattice dislocations through two $\Sigma 11$ tilt GBs in FCC aluminum. This demonstrates the complexity of dislocation–GB interactions, showing the activity of different atomic processes as a function of the glide plane of the impinging dislocation. Second, we consider the results of 3-dimensional (3D) simulations in which we observe slip transmission of dislocation loops nucleated from a crack tip near a series of different symmetric pure tilt GBs in FCC Ni. The trends of the results are then rationalized in terms of a simple line-tension (LT) model, suggesting that only three parameters are relevant in describing the slip transmission resistance of the GBs.

2. 2D atomistic simulations

2.1. Analysis of slip dislocation interaction with tilt grain boundaries

When slip dislocations collide with a GB there are three fundamental reactions that may take place. Assuming the slip dislocation is not repelled by the GB due to elastic interactions with other dislocations in the vicinity of the boundary or by image force effects, the dislocation may be absorbed, transmitted, or reflected. Each of these interactions changes the grain boundary in ways that depend on the character of the residual GB dislocations remaining after a particular reaction occurs. A slip dislocation can be absorbed by dissociating into a number of GB dislocations. Perfect GB dislocations are members of the displacement-shift-complete (DSC) basis set and the Burgers vectors of lattice dislocations can be expressed as linear combinations of the DSC basis. Another reaction involves a slip dislocation moving into a GB, while another lattice dislocation emerges into an adjacent grain, referred to as slip transmission. A residual dislocation remains in the boundary with a Burgers vector that is equal to the difference between the slip dislocation Burgers vectors. Specifically, the residual Burgers vector, $\vec{b}_{\mathrm{r}}$ is given by

$$\vec{b}_{\mathrm{r}} = \vec{b}_1 - R\vec{b}_2, \tag{1}$$

where $\vec{b}_1$ is the Burgers vector of the incident slip dislocation, $\vec{b}_2$ is the Burgers vector of the transmitted slip dislocation and R is the rotation matrix that characterizes the misorientation across the GB. It is conceivable that slip transmission could occur by a GB first absorbing a matrix dislocation, and then nucleating a lattice dislocation in the adjacent grain at a location remote from the original absorption site. This process would involve motion of GB dislocations and coalescence of those dislocations into an appropriate lattice dislocation. The third possible reaction involves reflection of an impinging lattice dislocation back into the original grain. This mechanism is believed to operate under conditions where there is significant resistance to absorption or transmission of lattice dislocations due to lack of favorably oriented glide planes in the neighboring crystal, the presence of obstacles such as hard particles, or elastic interaction stresses from dislocation pile-ups within the GB. As with the transmission case there is a residual dislocation remaining in the GB due to the reflection process.

To explore the details of slip dislocation interaction with GBs, conservation of Burgers vector analyses and 2D atomistic simulations were performed. Two GBs were selected for study, both belonging to the same $\Sigma 11$ coincident site lattice. One of the GBs is a $\Sigma 11\langle 1\,0\,1\rangle\{1\,3\,1\}$ symmetric tilt boundary and the other a $\Sigma 11\langle 1\,0\,1\rangle\{2\,5\,2\}|\{4\,1\,4\}$ asymmetric tilt boundary. The symmetric boundary is a low-energy boundary (0.13 J/m^2) with a simple structure, whereas the asymmetric boundary is a high-energy boundary with a complex and variable structure depending on the relative translation between the two grains. The asymmetric GB examined in this work deviated from the perfect CSL orientation by shifting the upper grain relative to the lower grain by 23.5 DSC vectors in the x-direction and half the repeat distance in the z-direction. This was found to be the

lowest energy configuration (0.38 J/m^2) for this GB. The crystallographic relationships for the symmetric and asymmetric GBs are depicted in Fig. 1(a) and (b), respectively.

The simplest slip dislocation–GB interaction for the $\Sigma 11$ symmetric boundary is transmission of the pure screw dislocation **DA**, $\frac{a}{2}[1\,0\,1]$, whose Burgers vector is parallel to the tilt axis. Conservation of Burgers vector analysis shows that no GB dislocations remain when the screw dislocation is transmitted. Because of this it is anticipated that transmission of the pure screw should be relatively easy compared to pure edge or mixed dislocations. If we assume that the pure screw is fully absorbed into the GB prior to any transmission events in the lower grain, then we find that the GB dislocations shown in Table 1 are produced. The first two rows in Table 1 show the GB dislocations produced when partials $\boldsymbol{\beta}$**A**, $\frac{a}{6}[1\,\bar{1}\,2]$, and **D**$\boldsymbol{\beta}$, $\frac{a}{6}[2\,1\,1]$, are absorbed. The third row is the net GB dislocation content after complete absorption of **DA**. This corresponds to the following dissociation reaction

$$\frac{a}{2}[1\,0\,1] \rightarrow \frac{a}{22}[3\,\bar{2}\,\bar{3}] + \frac{2a}{22}[4\,1\,7] \equiv \frac{a}{22}[4\,1\,7] + \frac{a}{22}[7\,\bar{1}\,4]. \tag{2}$$

The stacking fault energy for the dissociated configuration is zero since the faulted structure is the same as the perfect $\Sigma 11$ CSL configuration. Atomistic simulation results show that these GB dislocations are highly mobile and glide away from each other due to elastic repulsion [1]. Thus, the perfect screw dislocation is absorbed into the GB and no transmission occurs.

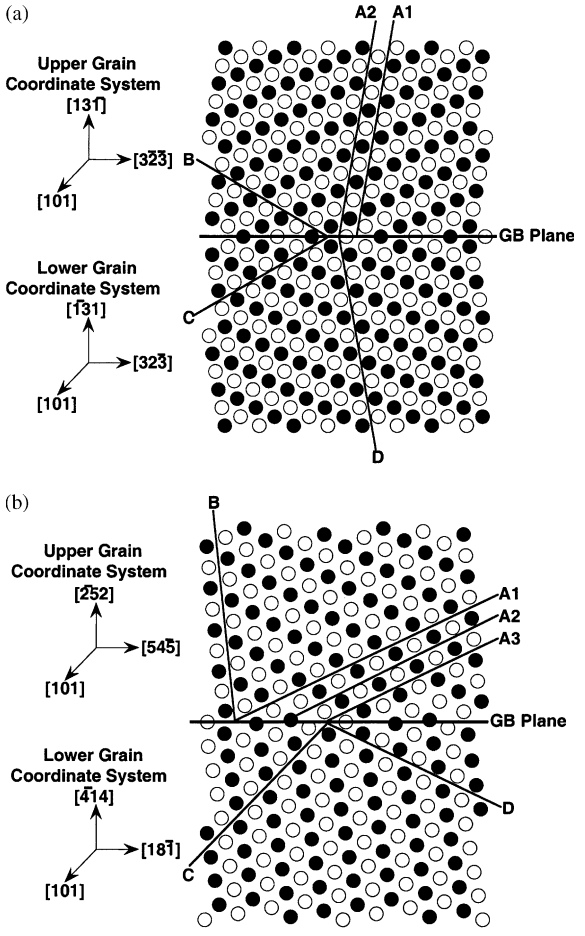

Fig. 1. (a) Orientation relationship for the $\Sigma 11\langle 1\,0\,1\rangle\{1\,3\,1\}$ symmetric tilt GB. (b) Orientation relationship for the $\Sigma 11\langle 1\,0\,1\rangle\{2\,5\,2\}|\{4\,1\,4\}$ symmetric tilt GB.

Two cases of dislocation transmission were examined in the symmetric $\Sigma 11$ GB and one case of reflection. The first dislocation transmission case involved **CA**, $\frac{a}{2}[0\,\bar{1}\,1]$, on plane A transmitted as **BA**, $\frac{a}{2}[1\,\bar{1}\,0]$, on plane D (see Fig. 1(a)). In the second case, **CA** on A transmits as **CA** on plane C. The conservation of Burgers vector results for both of these cases are presented in Table 1. Rows 4 through 8 show the GB dislocations produced when **CA** transmits as **BA** and rows 4, 5, 9, 10, and 11 present the results when **CA** transmits as **CA**. Note that a larger residual GBD is found when **CA** transmits on plane C, $(\frac{2a}{22}[3\,\bar{2}\,\bar{3}] + \frac{a}{22}[\bar{2}\,\bar{6}\,2])$, compared to transmission on D, $(\frac{a}{22}[\bar{3}\,2\,3])$. Consequently, the applied stress required for transmission on plane C should be greater than for transmission on plane D. We predict creation of $\frac{a}{22}[4\,1\,7]$ type GB dislocations occurs as partial dislocations are absorbed and emitted from the GB. Since these GBDs are mobile in the symmetric $\Sigma 11$ GB, the transmission process may be affected by their motion away from the intersection site. None of the other GB dislocations produced upon absorption or emission are mobile. The $\frac{a}{22}[2\,6\,\bar{2}]$ GBDs can only move by climb since their Burgers vector points out of the GB plane and the $\frac{a}{22}[3\,\bar{2}\,\bar{3}]$ is sessile since it is not a perfect GBD. In the case of glide dislocation reflection (**CA** is reflected as **BA** on plane B, see rows 4, 5, 12, 13 and 14 in Table 1) a somewhat larger residual GB dislocation is produced, $(\frac{3a}{22}[\bar{3}\,2\,3] + \frac{a}{22}[\bar{2}\,\bar{6}\,2])$, suggesting that this process may be more difficult than transmission.

One case of slip dislocation transmission was examined for the asymmetric $\Sigma 11$ GB. This involved the mixed dislocation **CA** on plane A transmitted as **BA** on plane C (see Fig. 1(b)). Conservation of Burgers vector results for this case are given in Table 2. Slip dislocation **CA** is initially absorbed and produces, among other GB dislocations, a $(\frac{9}{2})\frac{a}{66}[\bar{5}\,\bar{4}\,5]$ (see rows 1–3 in Table 2). This GBD is potentially mobile since its Burgers vector is parallel to the GB plane and it is a perfect GB dislocation. All of the other GB dislocations should be sessile including the residual GBDs (row 6, Table 2) remaining after transection.

Table 1
Continuum analysis of dislocation transmission processes for the symmetric Σ11 GB

Event	Grain boundary dislocations		
	$\frac{a}{22}[3\bar{2}\bar{3}]$	$\frac{a}{22}[26\bar{2}]$	$\frac{a}{22}[417]$
*Absorption of **DA** from plane A into GB*			
βA absorbed	$\frac{1}{3}$	$-\frac{2}{3}$	1
Dβ absorbed	$\frac{2}{3}$	$\frac{2}{3}$	1
GBDs	1	0	2
Absorption of CA from plane A into GB			
βA absorbed	$\frac{1}{3}$	$-\frac{2}{3}$	1
Cβ absorbed	$-\frac{1}{3}$	$-\frac{4}{3}$	0
*Transmission of **BA** to plane D*			
Bγ emitted	$-\frac{1}{3}$	$\frac{4}{3}$	0
γA emitted	$-\frac{2}{3}$	$\frac{2}{3}$	−1
Residual GBDs	−1	0	0
*Transmission of **CA** to plane C*			
Cβ emitted	$\frac{5}{3}$	$\frac{2}{3}$	0
βA emitted	$\frac{1}{3}$	$\frac{1}{3}$	−1
Residual GBDs	2	−1	0
*Reflection of **BA** to plane B*			
Bγ emitted	$-\frac{5}{3}$	$\frac{2}{3}$	0
γA emitted	$-\frac{4}{3}$	$\frac{1}{3}$	−1
Residual GBDs	−3	−1	0

Table 2
Continuum analysis of dislocation transmission processes for the asymmetric Σ11 GB

Event	Grain boundary dislocations		
	$\frac{a}{66}[54\bar{5}]$	$\frac{a}{33}[\bar{2}52]$	$\frac{a}{2}[101]$
*Absorption of **CA** from plane A into GB*			
βA absorbed	$-\frac{3}{2}$	$-\frac{1}{2}$	$\frac{1}{2}$
Cβ absorbed	−3	−1	0
GBDs	$-\frac{9}{2}$	$-\frac{3}{2}$	$\frac{1}{2}$
*Transmission of **BA** to plane C*			
Bγ emitted	$\frac{14}{6}$	$\frac{7}{6}$	0
γA emitted	$\frac{7}{6}$	$\frac{5}{6}$	$-\frac{1}{2}$
Residual GBDs	−1	1	0

2.2. Atomistic computational procedure

Most of the details pertaining to the methodology used in the calculations of the atomic arrangements of GBs have been described in detail elsewhere [1,2]. The model consists of a two part computational cell, rectangular in shape. One part, Region 1 contains movable atoms embedded in a semi-rigid part, Region 2. The GB approximately bisects the model as shown in Fig. 1. Equilibrium, $\sim$0 K, structures are obtained via relaxation using molecular dynamics with an energy quench. The two grains are free to move and undergo homogenous displacement in all three directions and this movement occurs during the relaxation via a viscous drag algorithm. Periodic boundary conditions were employed parallel to the z-direction, i.e. parallel to the tilt axis. An EAM interatomic potential was used in this study derived by Ercolessi and Adams [3] for Al.

2.3. Dislocations and quasi-static straining

Dislocations were introduced into the models by applying the fully anisotropic displacement field for a dislocation on an interface between two elastically dissimilar materials [4]. The dislocation lines were parallel to the tilt axis in all cases and the dislocations were placed on a suitable (1 1 1)-plane in the upper grain within a few lattice spacings of the boundary plane. In each case discussed here the same upper grain dislocation was introduced into the model, namely the **CA** dislocation on the $(1\,\bar{1}\,\bar{1})$-plane (plane A in Fig. 1(a)).

Straining of models was accomplished by applying a strain gradient tensor to the upper and lower grain atoms that was calculated to apply a force that would move the upper grain dislocation toward the boundary plane. A quasi-static straining method was used in which the models were strained in increments of 0.0005 or 0.001 and then relaxed, followed by repeated straining until an event was observed. The strain tensor was selected to apply an equal resolved glide force on a given outgoing dislocation as on the incoming one. In this manner, the system was biased toward a certain outcome. Using Hooke's law for the upper and lower grain coordinate systems it is straightforward to calculate the stress tensor in each grain given the strain tensor and then solve for the glide force acting on a specific dislocation. By carefully choosing the strain tensor, we were able to cause the incoming dislocation in the upper grain to transect the boundary and exit on either of two (1 1 1)-planes available in the lower grain.

We studied dislocation–GB interactions using quasi-static straining for both the symmetric and asymmetric $\Sigma 11$ boundaries. For the symmetric $\Sigma 11$ boundary there are two non-equivalent (1 1 1)-planes for a given (1 1 1) slip system based on the differences in atomic environment at the intersection of the (1 1 1)-plane and the boundary plane (see Fig. 1(a)). For example, the upper grain of the symmetric $\Sigma 11$ contains the $(1\,\bar{1}\,\bar{1})$-plane (plane A in Fig. 1(a)) and the $(\bar{1}\,\bar{1}\,1)$-plane (plane B). Each of these planes intersects the symmetric $\Sigma 11$ grain boundary in two different atomic environments, which corresponds to the period of the grain boundary in the x-direction. For the asymmetric $\Sigma 11$ boundary there are three different intersection environments (see Fig. 1(b)) for each of the upper grain $(1\,\bar{1}\,\bar{1})$-plane and six environments for each upper grain $(\bar{1}\,\bar{1}\,1)$-plane.

2.4. Simulation results

The results are summarized in Table 3 for the symmetric $\Sigma 11$ boundary and Table 4 for the asymmetric boundary. In general, it was possible to bias each system to observe the identical upper grain dislocation transect the boundary in many different ways, and it was observed that the local atomic environment played an important role in determining the outcome for identical strain tensors. For example, case 1 in Table 3 shows that an applied strain that places equal glide forces on an incoming **CA** dislocation on plane A and an outgoing **BA** dislocation on plane D (see Fig. 1(a)) such that these are the largest glide forces in the system causes **CA** to transect the boundary and form **BA** in the lower grain,

Table 3
Results of 2D straining simulations for symmetric $\Sigma 11$ GB

Case/incoming dislocation	Favored outgoing dislocation	Observed outgoing dislocation	Glide stress at transection (GPa)	Observations
1–1 **CA** on A-1	**BA** on plane D	**BA** on D	1.04	2 $\frac{a}{22}$[4 1 7] GB dislocations glide to right
1–2 **CA** on A-2	**BA** on plane D	**BA** on D	0.63	No $\frac{a}{22}$[4 1 7] observed
2–1 **CA** on A-1	**CA** on plane C	**CA** on C	1.6	No $\frac{a}{22}$[4 1 7] observed
2–2 **CA** on A-2	**CA** on plane C	**CA** on C	1.4	No $\frac{a}{22}$[4 1 7] observed
3–1 **CA** on A-1	**BA** on plane B	**BA** on D	No reflection, partial transection	1 $\frac{a}{22}$[4 1 7] GB dislocation glides to right
3–2 **CA** on A-2	**BA** on plane B	**BA** on B	1.25 (reflection)	2 $\frac{a}{22}$[4 1 7] GB dislocations glide to right

Table 4
Results of 2D straining simulations for asymmetric Σ11 GB

Incoming dislocation	Favored outgoing dislocation[a]	Observed outgoing dislocation	Glide stress at transection (GPa)	Observations
1–1 **CA** on A-1	**BA** on plane C	**BA** on C	1.34	GB dislocation? Glides to right
1–2 **CA** on A-2	**BA** on plane C	**CA** on D	1.45	GB dislocation? Glides to right, GB facets, **CA** appears 6 planes to left of plane of intersection
1–3 **CA** on A-3	**BA** on plane C	**CA** on D	1.49	GB dislocation? Glides to right, GB facets, **CA** appears 6 planes to left of plane of intersection
2–1 **CA** on A-1	**BA** on plane C	**BA** on C	2.25	No GB dislocations until transection, **BA** appears 2 planes to left of plane of intersection
2–2 **CA** on A-2	**BA** on plane C	**BA** on C	1.52	No GB dislocations, **BA** appears 2 planes to left of plane of intersection
2–3 **CA** on A-3	**BA** on plane C	**BA** on C	2.11	No GB dislocations until transection, **BA** appears on plane of intersection

[a] Strain tensor modified from case 1 to 2 to reduce glide force for **CA** on plane D.

which then glides away into the lower grain. However, case 1 consists of two sub-cases depending on which of two non-equivalent upper grain glide planes contains the incoming **CA** dislocation, case 1–1 and 1–2.

Case 1–1 corresponds to **CA** gliding on A-1, while case 1–2 corresponds to **CA** on A-2 and the results differ. For case 1–1 it is observed that at an applied strain of 0.003 (or 208 MPa on outgoing **BA**) that a mobile grain boundary dislocation, $\frac{a}{22}[4\,1\,7]$, is emitted at the intersection of the leading partial dislocation (**βA**) and the grain boundary, as predicted by the continuum analysis in Table 1. This dislocation is observed to glide in the boundary to the right edge of the model, where it is pinned. Further, the lower grain dislocation (**BA**) gradually emerges starting with the leading partial dislocation (**Bγ**) at an applied strain of 0.004. We observe that **Bγ** glides away from the boundary until a critical strain of 0.015 is reached and the trailing partial is created. This results in the release of an $-\frac{a}{22}[4\,1\,7]$, which also glides in the boundary to the right edge of the model. A residual GB dislocation $-\frac{a}{22}[3\,\bar{2}\,\bar{3}]$ is then observed to remain in the boundary at the point of transection, as predicted. Thus, boundary transection is accomplished at an applied strain of 0.015 for this case, which corresponds to a resolved glides stress of 1.05 GPa on **BA**, the outgoing dislocation, and 1.02 GPa on **CA**, the incoming dislocation.

However, the results are different for case 1–2, which corresponds to **CA** on A-2, but is otherwise identical. For this case, no mobile $\frac{a}{22}[4\,1\,7]$ dislocations are observed, Bγ appears in the lower grain at an applied strain of 0.005, and **BA** appears in the lower grain and glides away at an applied strain of 0.009. An identical residual grain boundary dislocation, $-\frac{a}{22}[3\,\bar{2}\,\bar{3}]$, remains in the boundary but transection occurs at a lower applied strain and at a correspondingly reduced glide stress of 0.63 GPa on **BA** and **CA**. Other variations are noted in Tables 3 and 4.

Particularly interesting are the observations that (1) otherwise identical inputs can result in grain boundary transection by different outgoing dislocations, such as case 3–1 and 3–2 for the symmetric boundary and cases 1–1, 1–2, and 1–3 for the asymmetric boundary, (2) the critical resolved glide stress varies in transmission, and (3) the transmitting dislocation does not always appear on the slip plane that intersects the incoming slip plane. We also note that the asymmetric boundary, on average, appears to be harder to transect compared to the symmetric boundary.

3. Modeling GB resistance to dislocation slip transmission in FCC Ni

3.1. Atomistic simulations

Using molecular dynamics (MD) simulations we observe the behavior of dislocations impinging on grain boundaries in FCC Ni, as described by an embedded-atom model [5]. As a particular case study, we focus on the outcomes of dislocation–GB collisions for six symmetric tilt boundary geometries. For this purpose computational cells containing approximately 1.2×10^6 atoms are divided into two crystalline grains separated by the tilt boundary. The GBs are created by rotating grain 1 over an angle 2α about their common $[0\,0\,\bar{1}]$ crystallographic axis, while the normal to the GB plane is obtained by rotating a unit vector in the $[\bar{1}\,1\,0]$ direction of

grain 1 over an angle α about the $[00\bar{1}]$ axis. In order to provide a dislocation source near the GB plane, a crack is introduced along the $[\bar{1}10]$ direction of grain 1.

Each simulation is initiated from a zero-temperature, relaxed GB/crack configuration. Subsequently, the computational cell is strained perpendicular to the crack plane at a constant rate, keeping the cell dimensions fixed along the other two directions. Under the influence of the increasing uniaxial strain in the system, dislocation loops are nucleated at the crack tip, followed by their expansion under stress, eventually reaching the GB plane. The peak shear stress level reached during this stage was estimated to be of the order of 5 GPa. Such high values were necessary to incite sufficient dislocation activity over the short time intervals typical of the MD simulations ($\sim$100 ps). In order to restrict the number of dislocation loops in the cell, the strain rate is reduced to zero after the nucleation of the first few loops, after which the simulation continues at a constant volume.

3.2. Line-tension model

In order to analyze the role of the various geometrical parameters in the trend of the atomistic observations we exploit the results within the framework of a simple line-tension model. The model represents a case study in which we investigate how the activation conditions of a Frank–Read (FR) source, a dislocation segment pinned between two points separated by distance L, are affected by the presence of a grain boundary within the isotropic line-tension (LT) approximation [6]. Within this framework, dislocation segments are treated as elastic bands that interact only with external stresses. Assuming that the energy per unit length of dislocation is independent of its direction, the self-interaction is accounted for through a constant line-tension factor γ that depends only on the magnitude of the Burgers vector b.

In the absence of internal obstacles such as a GB, the pinned dislocation segment bows out in response to the local resolved shear stress τ. For values of τ smaller than the critical stress the segment evolves towards an equilibrium configuration formed by a circular arc with radius of curvature r in which the LT restoring forces balance the applied stress. This configuration corresponds to the minimum of the LT energy function

$$U(r) = \gamma l(r) - \tau b A_{\mathrm{SW}} \tag{3}$$

given by the elastic line energy of the dislocation segment minus the work done by the resolved stress τ. Here, $l(r)$ is the length of the curved dislocation segment and A_{SW} is the corresponding swept area in the glide plane. When the applied stress τ exceeds the critical value

$$\tau^0_{\mathrm{crit}} = 2\gamma/bL \tag{4}$$

the energy function in Eq. (3) no longer possesses a stable minimum, implying source activation.

In the presence of an internal obstacle such as a GB, the conditions for activation of a FR source are expected to be different. Given that the expansion of the dislocation segment is obstructed by the GB, the critical stress required to activate the source may be different from the reference value in the absence of any internal constraints. In the present study we consider this confinement effect for the case in which a FR source of length L and Burgers vector $\vec{b}_1$, is placed in grain 1 at a distance d parallel to a GB plane separating grains 1 and 2, as shown in Fig. 2. Within the LT model we assume that both grains are elastically isotropic, the GB has no internal structure, and the LT energy factor depends only on the magnitude of the Burgers vector of the segment under consideration. As in the unconstrained case, the critical conditions for activation in this situation are determined by examining the stability of the appropriate LT internal energy expressions. Similar to the unconstrained case, these expressions involve energy contributions due to elastic line energy of the dislocation segments as well as terms describing the work done by the resolved stresses. However, for the constrained source, a number of additional parameters naturally enter the equations. Considering a given pair of incoming (grain 1) and outgoing (grain 2) slip systems, the energy expressions involve the two corresponding resolved shear stresses τ_1, and τ_2, a residual Burgers vector Δb which describes the magnitude of the residual

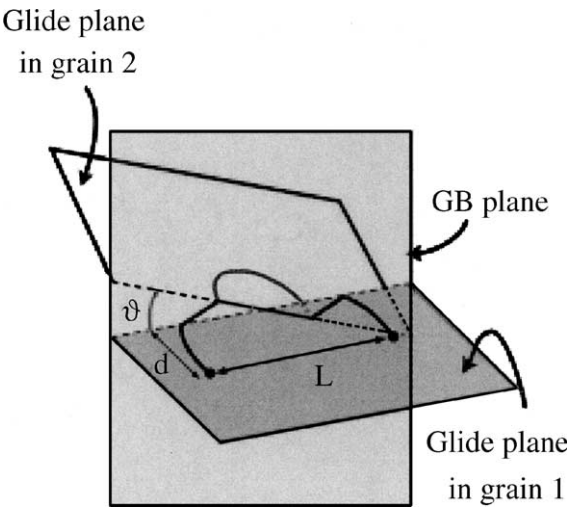

Fig. 2. Activation of a source from grain 1 into grain 2. Generally, the incoming and the outgoing slip planes intersect each other in the boundary at a non-zero angle ϑ. It is assumed that, in order to accommodate this misorientation the residual dislocation forms a junction configuration in the boundary plane. See [7] for details.

Table 5
Comparison of MD simulation observations for six different GB configurations with slip transmission resistances determined using our LT model for FR source at standoff distance ratios of $d/L = 0.1$, 0.3, and 0.4

Σ	α, °	d/L			MD Observtions
		0.1	0.3	0.4	
13	11.31	1.19	1.35	1.37	Many slip transmission (ST) events
65	15.25	1.76	1.56	1.54	Few ST events
5	18.43	2.36	1.78	1.71	Few ST events
29	21.80	3.11	2.07	1.94	No ST
17	30.96	4.73	2.25	1.99	No ST
5	26.57	5.31	2.40	2.06	No ST

Burgers vector left behind in the GB plane to comply with total Burgers vector conservation, and the angle ϑ shown in Fig. 2, describing the angle between the traces of the incoming and outgoing slip planes in the GB plane. In addition, we compare two distinct modes of activation. The first involves activation of configurations in which the expanding dislocation segment penetrates into grain 2, as shown in Fig. 2. The second concerns the situation in which the dislocation segment does not penetrate into grain 2 and slip propagation is restricted to grain 1. Considering these two scenarios, the critical stress for activation of the FR source in the presence of the GB for a given pair of incoming and outgoing slip systems is defined as the lowest resolved stress for which either of them is activated. For full details, see Ref. [7].

Using the LT model it is now straightforward to determine the source activation condition for each of the 144 pairs of incoming/outgoing slip systems. These stress values can be regarded as a 12×12 slip transmission matrix, each element of which contains the critical source activation stress for a given combination of incoming and outgoing slip systems. In order to make a connection to the MD results in the previous section, we used the LT model to compute the slip transmission stress for each of the 144 pairs of slip systems and for each of the six tilt boundaries considered in the atomistic simulations. For this purpose, we evaluated the intersection angles ϑ, residual Burgers vector Δb and resolved shear stress ratio τ_2/τ_1, for each of the 12×12 pairs of incoming and outgoing slip systems and for each of the six symmetric tilt boundaries examined in the MD simulations. Using these parameters as input to the LT model, we computed the critical activation stresses for each of the 144 pairs of slip systems in each GB for three different values of the standoff distance ratio $d/L = 0.1$, 0.3 and 0.4, respectively. Since the absolute values of the LT critical stresses depend on the chosen value of d/L, they have no strict quantitative meaning in relation to the MD simulations. However, their values do provide a measure of the relative slip transmission resistance among all possible pairs of incoming and outgoing slip systems for a given combination of GB geometry and applied stress. Assuming that the lowest among them is a measure of the slip transmission resistance of the GB in question under the considered loading conditions, we ranked the six boundaries in the order of their minimal transmission stress, from the lowest to the highest, for each of the values of d/L considered. The results are presented in Table 5, along with the slip transmission observations from the MD simulations. Although the absolute values of the LT slip transmission resistances are seen to be quite different among the three values of d/L, it is clear that for each value of d/L the *relative* ranking of the six GBs within the LT model is in line with the MD results. In each case, the GB with the lowest LT critical stress shows most slip transmission events in the MD simulations, whereas the GBs with the highest resistances show no slip transmission in the atomistic calculations.

These results and the fact that the empirical slip transmission rules deduced from in situ TEM observations reported in Refs. [8–10] involve the exact same parameters indicate that, despite its rather crude nature, the LT model captures some of the essential energetics of dislocation slip transfer across GBs. The parameter space governing this mechanism does not seem so terrifyingly complicated as it is usually assumed and the model suggests relatively simple functional relationships between the GB geometry and loading conditions on one hand, and slip transmission stress on the other. However crude, these relationships identify targets for a more accurate parameterization of slip transmission conditions that can be used in the quantitative modeling of the plasticity mechanisms at the microscale.

4. Discussion and summary

This paper describes 2D and 3D simulations of GB–dislocation interactions that can be used to understand

the unit mechanisms involved in dislocation absorption, transmission, and reflection and may help determine which parameters need to be passed up to higher length and time scales in a multiscale paradigm. The richness of the GB–dislocation problem is daunting and these results provide direct evidence of that complexity. The 2D results show that a range of outcomes from otherwise identical inputs can be observed for certain geometries that may or may not agree with elastic analyses. This is not surprising since the latter does not capture the full atomic structure of a GB. However, these results point out weaknesses in our understanding of these problems since we cannot yet explain why the simulation outcomes should differ from this simple analysis for a given simulation case shown here. For example, we do not yet understand why we observe formation of $\frac{a}{22}[4\,1\,7]$ GB dislocations when **CA** penetrates the $\Sigma 11$ symmetric tilt GB when it lies on plane A-l but not on plane A-2 (Table 3). Continuum elasticity analysis remains mute in this regard. We assume that an explanation lies at a deeper level, perhaps involving details of gamma surface differences where the GB plane intersects planes A-1 and A-2.

Analysis of the transmission of **CA** through the $\Sigma 11$ asymmetric GB is more involved and we observe that transmission does not always occur on the favored outgoing slip plane. We know from the structure of the asymmetric GB that incoming and outgoing slip planes are not 'continuous' in the same way as for the symmetric GB so this result is not entirely unexpected. However, we need to understand the Burgers vectors of the GB dislocations that form during transmission of **CA** as our initial atomic disregistry analysis indicates that the GB may be restructuring as a GB dislocation glides along the boundary to the right (Table 4).

Comparing transection stresses for the symmetric and asymmetric boundaries reveals that the symmetric $\Sigma 11$ GB has lower energy pathways for transmission that are related to the ease with which GB dislocations can form on the boundary and related to the continuity of the $\{1\,1\,1\}$-planes across the boundary plane. However, the lowest transection stress occurs for the symmetric GB case where no GB dislocations form. This is related to maintaining a compact dislocation core structure at the transmission saddle point configuration. A more open boundary and/or the formation of glissile GB dislocations lend themselves to core spreading, which increases the transection stress.

Exploration of the 3D aspects of dislocation – GB collisions remains a challenge. Our preliminary results presented in this contribution indicate that, despite the daunting complexity of the situation, it appears possible to identify a set of simple geometrical parameters that correlate well with in situ TEM experimental observation of slip transmission in FCC metals [8–10]. The line-tension model presented here is an attempt to relate the outcomes of such collisions to the boundary geometry and local stress, completely ignoring boundary structure and possible interactions between lattice and grain boundary dislocations. On the other hand, the 2D analysis presented here shows that an accurate description demands thorough examination of grain boundary structure and possible dislocation reactions. In that sense, the structure-less analysis in 3D and the fully atomistic analysis of dislocation reactions in 2D complement each other and provide a viable approach for a comprehensive investigation of grain boundary effects in crystal plasticity.

Acknowledgements

This work was performed under the auspices of the US Department of Energy by the University of California, Lawrence Livermore National Laboratory under Contract no. W-7405-Eng-48. At PNNL the US Department of Energy, Office of Basic Energy Sciences, Materials Sciences and Engineering and Office of Fusion Energy Sciences supported this research under contract DE-AC06-76RLO1830. M.dK., R.J.K., V.V.B., C.H.H., W.C., and M.N. acknowledge support from the Computational Materials Science Network, Office of Basic Energy Sciences, the US Department of Energy.

References

[1] R.J. Kurtz, R.G. Hoagland, J.P. Hirth, Philos. Mag. A 79 (1999) 665.
[2] R.J. Kurtz, R.G. Hoagland, J.P. Hirth, Philos. Mag. A 79 (1999) 683.
[3] P. Ercolessi, J.B. Adams, Europhys. Lett. 26 (1994) 583.
[4] D.M. Barnett, J. Lothe, J. Phys. F. Met. Phys. 4 (1974) 1618.
[5] D.J. Oh, R.A. Johnson, J. Mater. Res. 3 (1988) 471.
[6] J.P. Hirth, J. Lothe, Theory of Dislocations, Krieger Publishing Company, Malabar, Florida, 1992, p. 174.
[7] M. de Koning, R. Miller, V.V. Bulatov, F.F. Abraham, Philos. Mag. A 82 (2002) 2511.
[8] Z. Shen, R.H. Wagoner, W.A.T. Clark, Acta Metall. 36 (1988) 3231.
[9] T.C. Lee, I.M. Robertson, H.K. Birnbaum, Scr. Metall. 23 (1989) 799.
[10] W.A.T. Clark, R.H. Wagoner, Z.Y. Shen, T.C. Lee, I.M. Robertson, H.K. Birnbaum, Scr. Metall. 26 (1992) 203.